Supporting Information

Sr/Ho-codoped $(K_{0.5}Na_{0.5})NbO_3$ photochromic-transparent ceramics in non-destructive optical data storage and multi-modal anti-counterfeiting

Fangyuan Yu,[a,1] Lixiang Deng,[a,1] Yan Chen,[a] Ping Zhou,[a] Xiao Wu,*[a] Cong Lin,[a] Chunlin Zhao,[a] Min Gao,[a] Tengfei Lin,[a] Laihui Luo[b] and Qiwei Zhang[c]

[a] Department of Material Science and Engineering, Fuzhou University, Fuzhou, 350108, China.

[b] Department of Microelectronic Science and Engineering, Ningbo University, Ningbo, 315211, China

[c] College of Physics and Technology, Guangxi Normal University, Guilin, 541004, China.

[1] F. Yu and L. Deng contributed equally to this work.

E-mail: wuxiao@fzu.edu.cn (Xiao Wu).

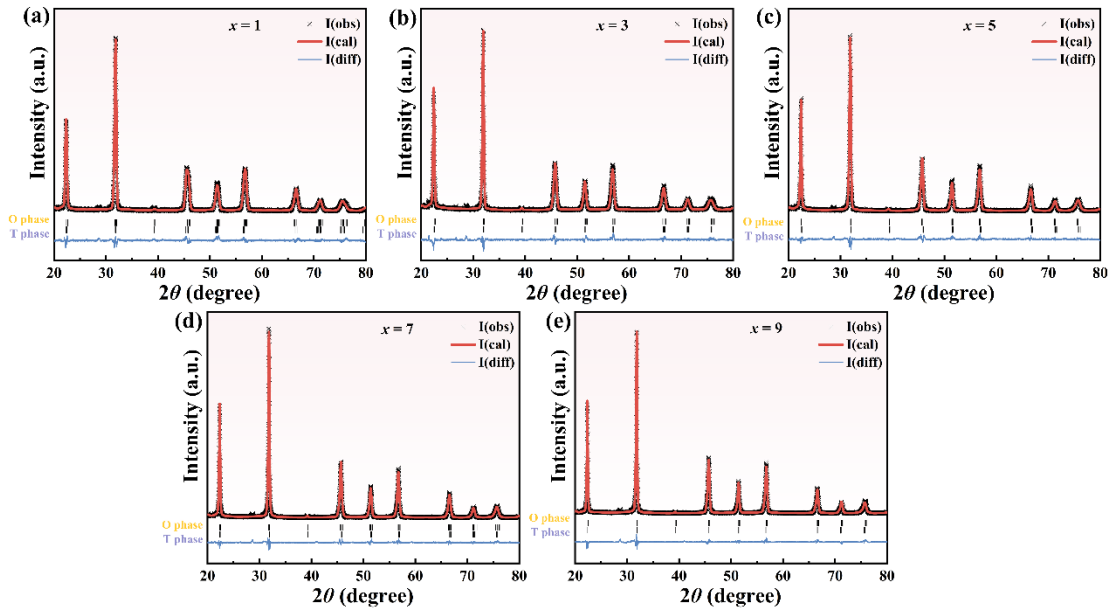

Figure S1 Rietveld refinement XRD patterns of the *x*Sr-1Ho-KNN ceramics, (a) $x = 1$, (b) $x = 3$, (c) $x = 5$, (d) $x = 7$ and (e) $x = 9$.

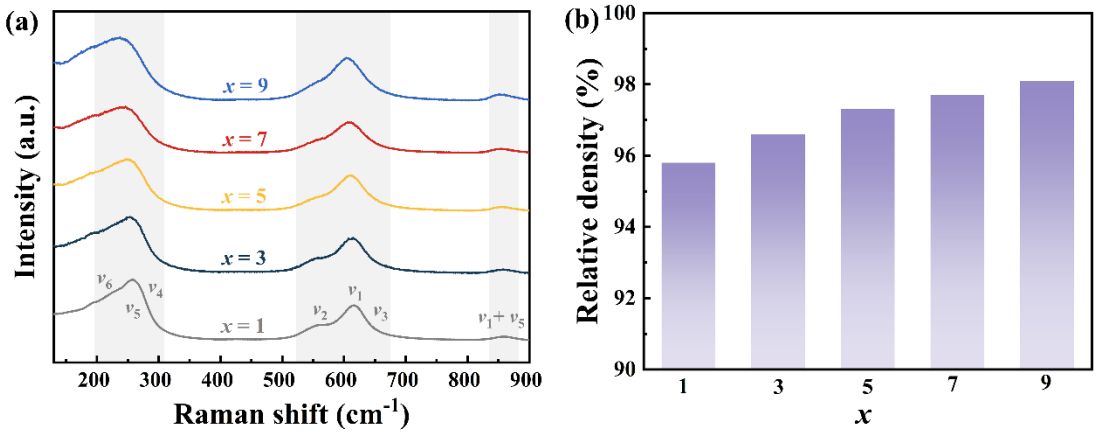

Figure S2 (a) Raman spectra and (b) relative density of the *x*Sr-1Ho-KNN ceramics (*x* = 1, 3, 5, 7, 9).

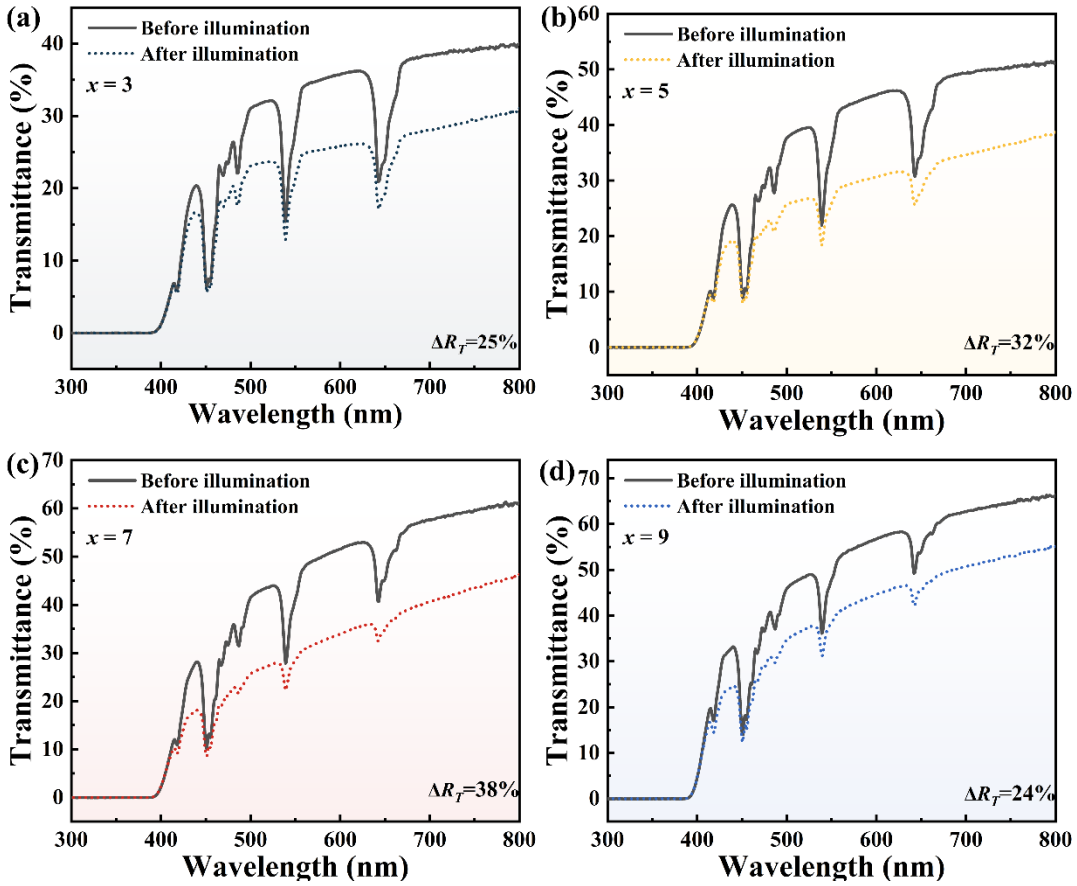

Figure S3 Optical transmittances of the *x*Sr-1Ho-KNN ceramics before and after illumination (for 10 s), (a) $x = 3$, (b) $x = 5$, (c) $x = 7$ and (d) $x = 9$.

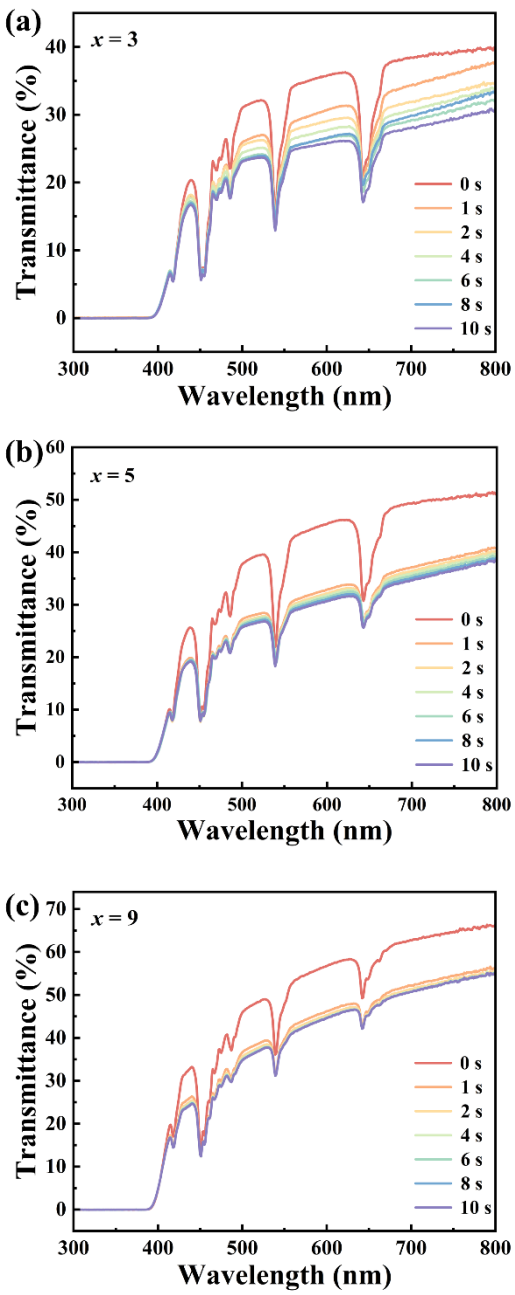

Figure S4 Transmittance values at 500 nm of the *x*Sr-1Ho-KNN ceramics at different illumination times, (a) $x = 3$, (b) $x = 5$ and (c) $x = 9$.

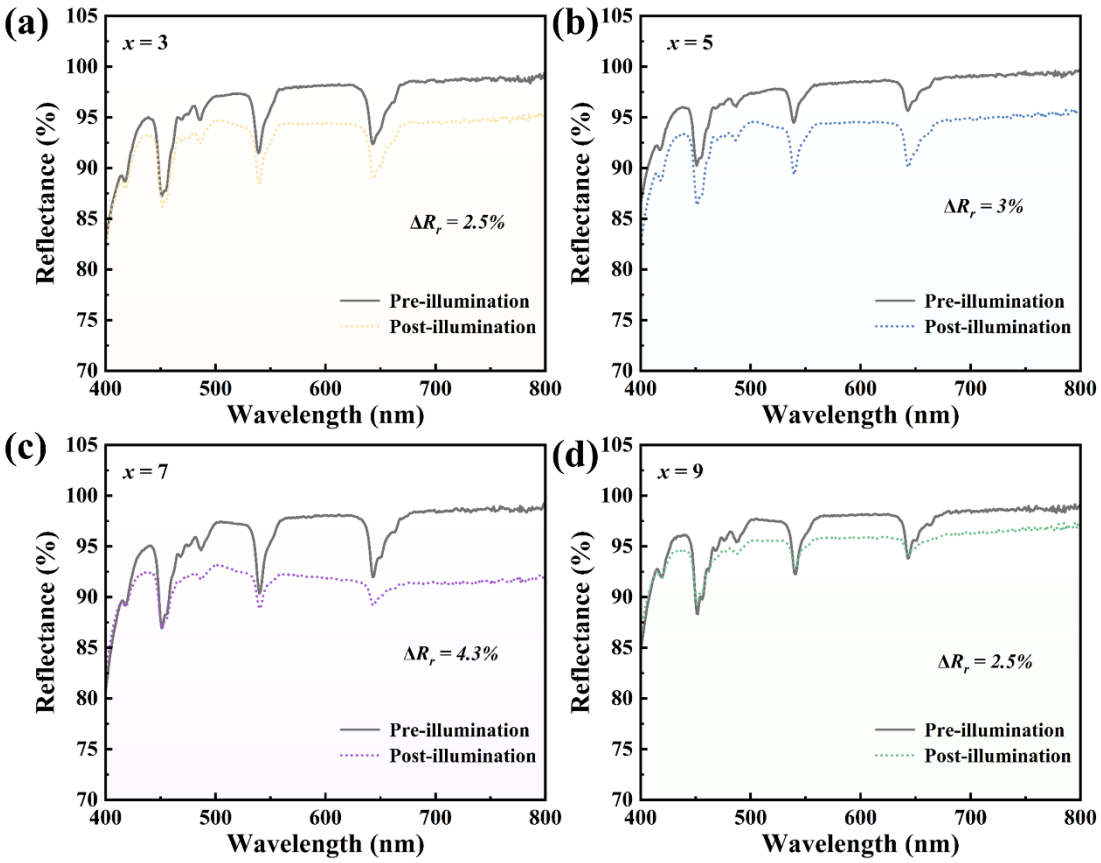

Figure S5 Diffuse reflectance spectra of the *x*Sr-1Ho-KNN ceramic powders before and after illumination (for 10 s), (a) $x = 3$, (b) $x = 5$, (c) $x = 7$ and (d) $x = 9$.

The measured reflectance contrasts (ΔR_r) of the *x*Sr-1Ho-KNN (x = 3, 5, 7, 9) ceramic powders are 2.5%, 3%, 4.3%, and 2.5%, respectively. This change trend aligns with that of the transmittance contrast (ΔR_T) of bulk ceramics, with 7Sr-1Ho-KNN consistently demonstrating the highest ΔR_T of 38%. However, the significantly lower ΔR_r values observed in powdered samples can be attributed to strong multiple scattering, which effectively reduce the excitation depth and diminish cumulative electron trapping at defect sites. In contrast, the high transparency (e.g., 60.7%) and extended optical path length in bulk ceramics improve photon-defect interactions, thereby enhancing ΔR_T.

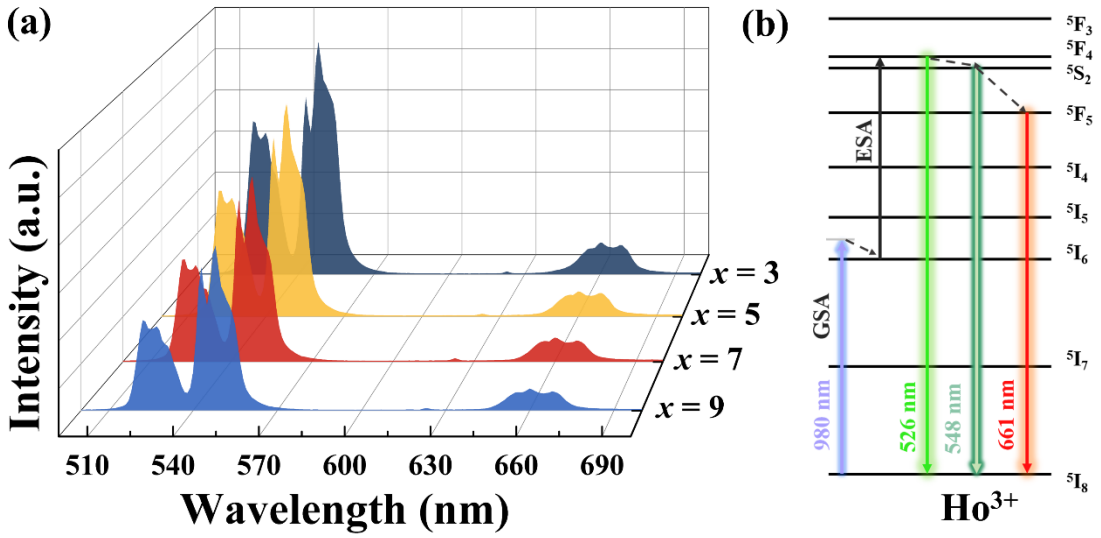

Figure S6 (a) UCPL spectra of the *x*Sr-1Ho-KNN ceramics. (b) Energy level diagram of Ho^{3+} in the ceramics and possible electronic transition mechanism.

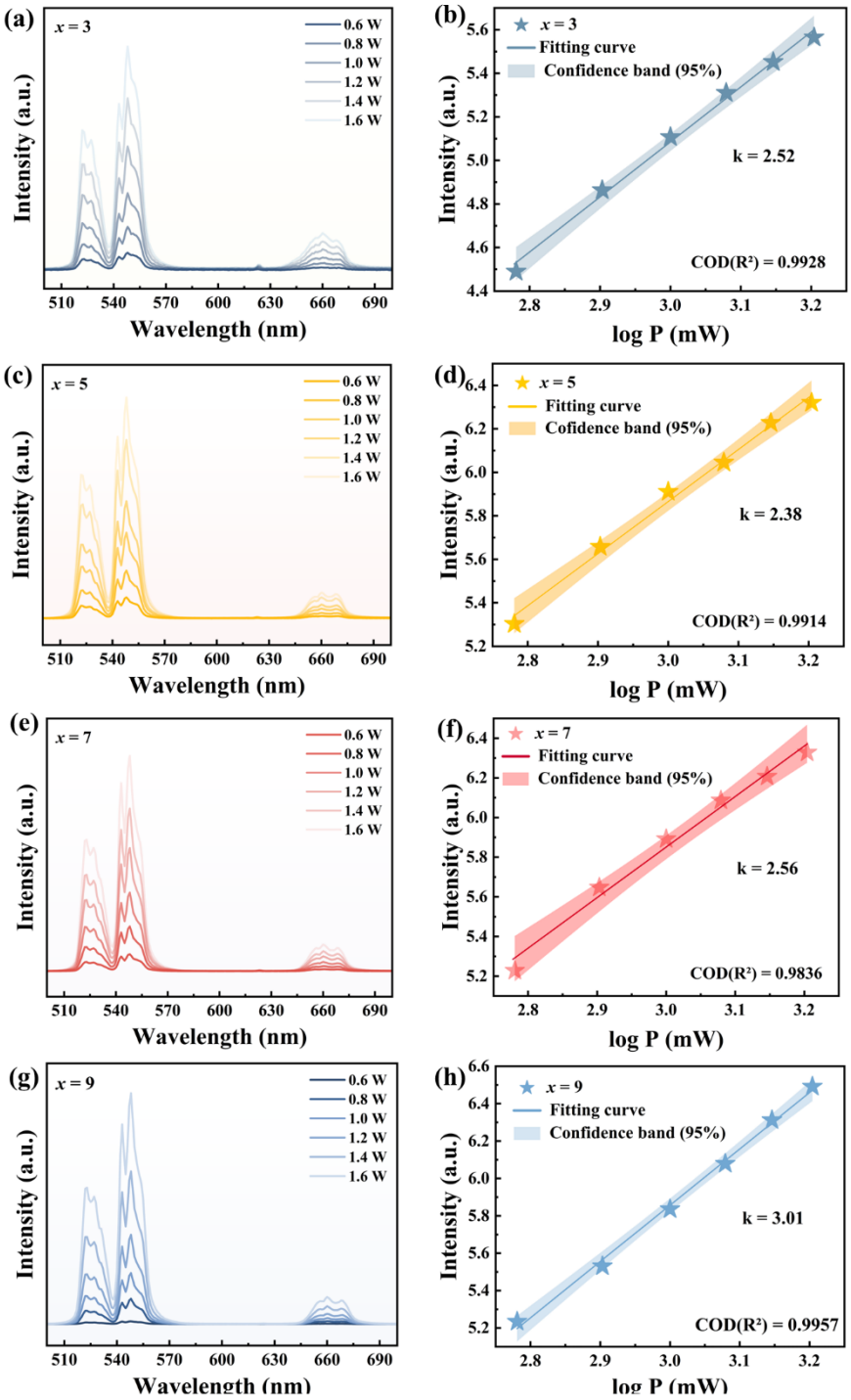

Figure S7 (a, c, e, g) UCPL spectra and (b, d, f, h) photon number fitting curves of the *x*Sr-1Ho-KNN ceramics under the excitation of 980-nm laser at different powers.

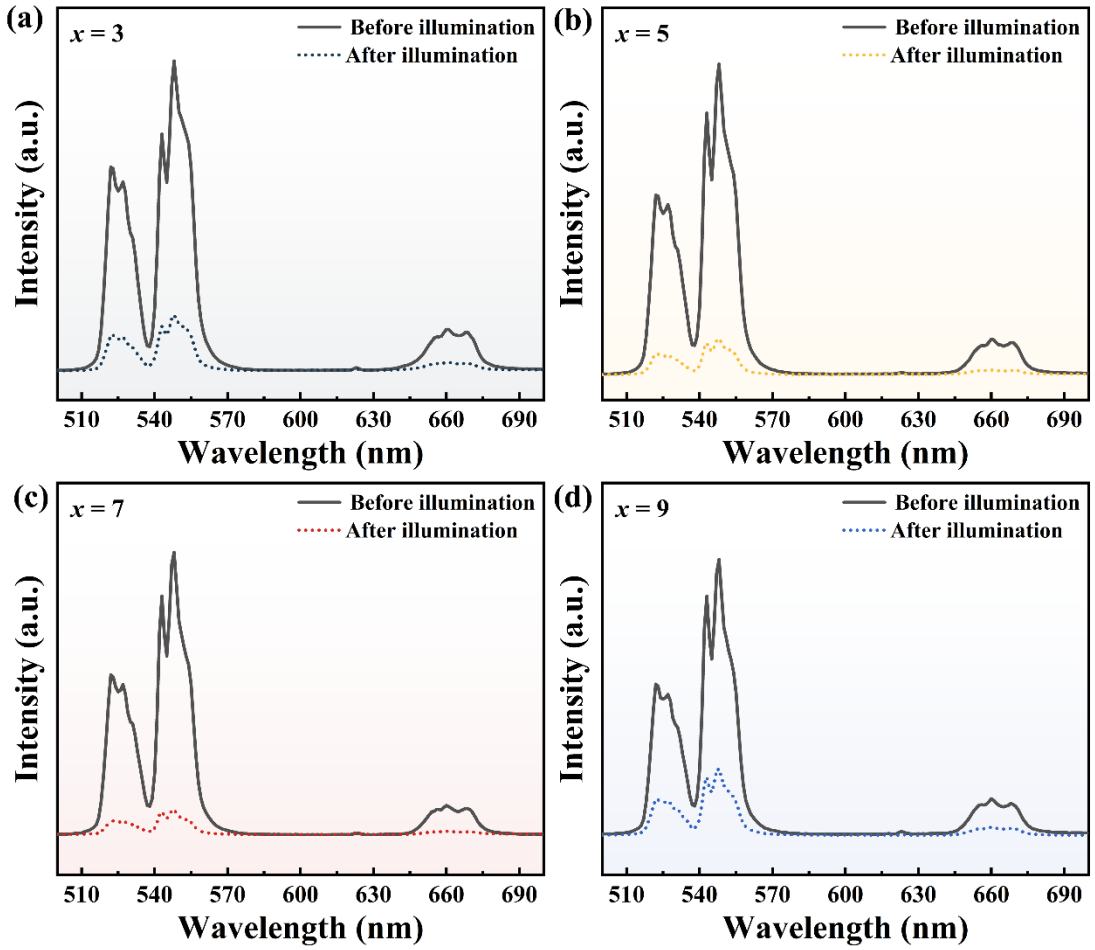

Figure S8 UCPL spectra (λ_{ex} = 980 nm) of the xSr-1Ho-KNN ceramics before and after illumination with 405 nm laser for 10 s, (a) x = 3, (b) x = 5, (c) x = 7 and (d) x = 9.

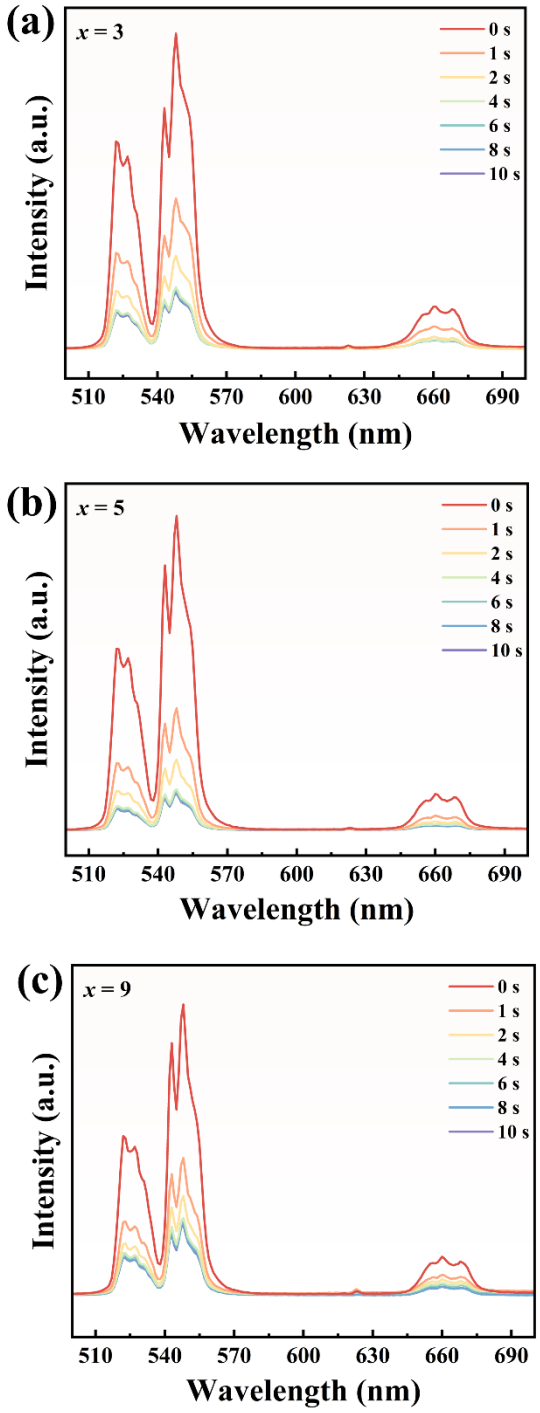

Figure S9 UCPL spectra of *x*Sr-1Ho-KNN ceramics (λ_{ex} = 485 nm) after being irradiated with a 405-nm laser for different time periods, (a) x = 3, (b) x = 5 and (c) x = 9.

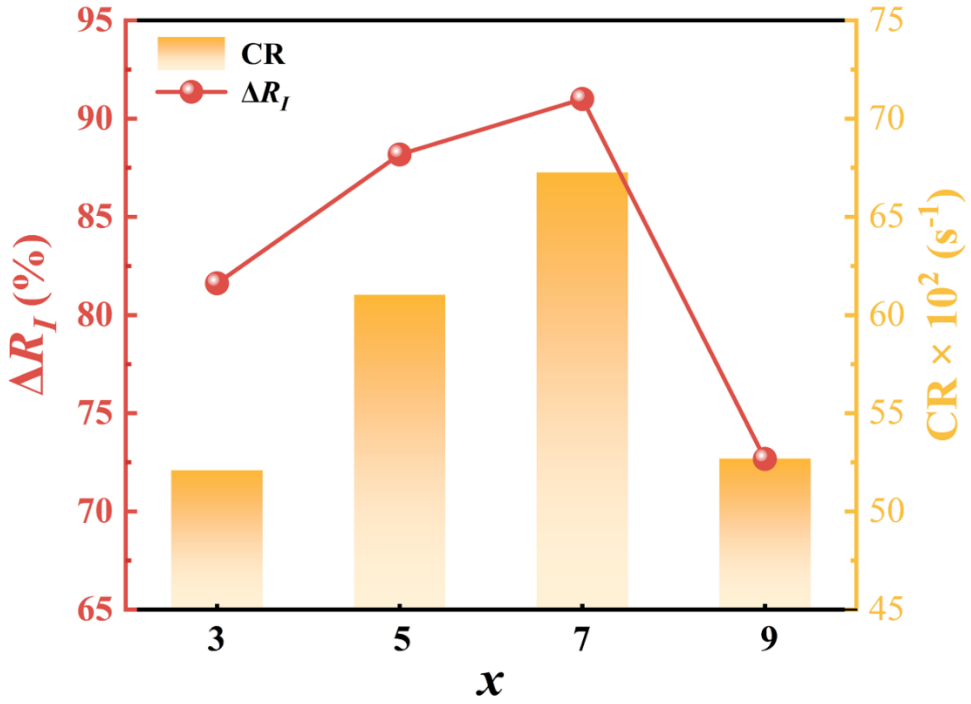

Figure S10 $^{\Delta R_I}$ and CR of the *x*Sr-1Ho-KNN ceramics.

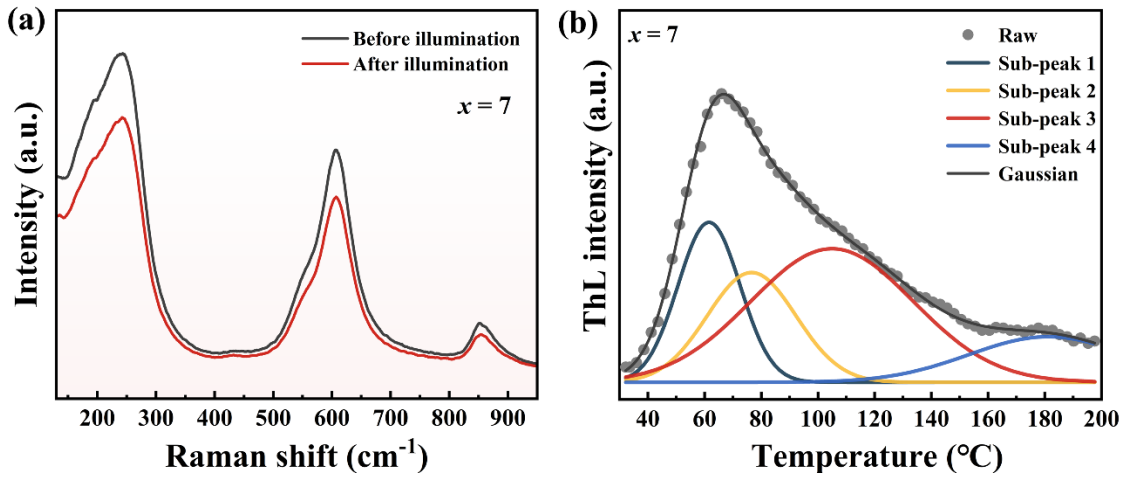

Figure S11 (a) Raman curves and (b) Gaussian fitting curves of the ThL curve before and after illumination of the 7Sr-1Ho-KNN ceramic.

Table S1 Lattice parameters and error factor (R_w) of the *x*Sr-1Ho-KNN ceramics.

Sample	Phase	Lattice parameters				c/a	R_w (%)
		a (Å)	b (Å)	c (Å)	ratio (%)		
$x = 1$	O	3.9464	5.6187	5.6523	64.90	1.1323	6.83
	T	3.9727	3.9727	4.1165	35.10	1.0362	
$x = 3$	O	3.9465	5.6201	5.6350	57.70	1.4278	7.56
	T	3.9703	3.9703	3.9842	42.30	1.0035	
$x = 5$	O	3.9821	5.6205	5.6174	31.43	1.4107	7.69
	T	3.9642	3.9642	3.9744	68.57	1.0026	
$x = 7$	O	3.9491	5.6305	5.6294	30.59	1.4255	6.79
	T	3.9647	3.9647	3.9750	69.41	1.0026	
$x = 9$	O	3.9630	5.6206	5.6188	28.78	1.4178	7.37
	T	3.9792	3.9792	3.9814	71.22	1.0006	